

Supporting Information

High-efficiency Absorption and Acoustic–electric Conversion in Heterogeneous Nanofibers: A Two-pronged Approach to Full-frequency De-noise

Supporting Information contains:

Supplementary Notes

Supplementary Fig. S1-10

Supplementary Table S 1- 4

Molecular dynamics simulations

The GRMOACS 2020.6 package was used for the molecular dynamics simulations.¹ VMD software was used to visualize the structures² Using the PACKMOL package, the molecules were mixed in a cubic box with periodic boundary conditions.³ The molecular number is shown in Table S1:

Table S1 The initial configuration setup for the simulation system.

System	PAN (15)	CNC (10)	DMF
	75	2	6000

The Generation Amber Force Field (GAFF)⁴ was chosen for this work because it is useful for investigating numerous tiny organic compounds.⁵⁻⁷

The initial configurations were relaxed with a conjugate gradient minimization approach before the MD simulation was initiated. The cycle was set to 5000 steps, and the step size was 0.01 nm. When the minimum force was less than $100 \text{ kJ} \cdot \text{mol}^{-1} \cdot \text{nm}^{-1}$, convergence was declared in the minimization. The cut-off approach was used to determine the van der Waals interaction, while the

PME (particle mesh Ewald) method was used to calculate the atomic electrostatic interaction, and both distances were 1.0 nm.⁸ The system was then equilibrated at 1.0 bar pressure to produce the appropriate density. The pressure and temperature were controlled using the Berendsen and V-rescale methods. The time constant was 1.0 ps, and the compressibility was $4.5 \cdot 10^{-5} \text{ bar}^{-1}$. The equilibrium was 5 ns for all systems with a 0.001 ps time step. Finally, the production ran for 50 ns. In the production run, the pressure control was altered to the Parrinello-Rahman method. The LINCS (Linear Constrain Solver) algorithm⁹ was also used to impose constraints on the hydrogen bond.

Sound pressure and acoustic impedance simulations

To forecast the relationship between the structure and properties of films, a suitable underlying theory of noise absorption properties is required. The Delany-Bazley (DB) model and the Johnson-Chamoux-Allard (JCA) model are now the most extensively used prediction models for porous materials.^{10,11} Because the DB model only has one independent variable, airflow resistance, it cannot directly guide the modulation of the porous material's internal microstructure (density, tortuosity, etc.). The JCA model, on the other hand, is the most often used model for predicting the noise absorption properties of porous materials. The noise absorption of porous material in this model is mostly due to the viscosity effect and the temperature effect, which are described by equivalent density (ρ_{eq}) and equivalent bulk modulus (K_{eq}), respectively. The following are the calculating formulas:

$$\rho_{eq}(\omega) = \frac{\alpha_{\infty} \rho_0}{\varphi} \left(1 + \frac{\sigma \varphi}{i \omega \alpha_{\infty} \rho_0} \sqrt{1 + \frac{4i \alpha_{\infty}^2 \eta \rho_0 \omega}{\sigma^2 \Lambda^2 \varphi^2}} \right)$$

(1)

$$K_{eq}(\omega) = \frac{\gamma\rho_0}{\varphi}[\gamma - (\gamma - 1)\left(1 + \frac{8\eta}{i\Lambda^2 P_r \omega \rho_0 \sqrt{1 + \frac{i\rho_0 \omega P_r \Lambda'^2}{16\eta}}}\right)^{-1}]^{-1}$$

(2)

Based on the Eqs (1) and (2), the characteristic impedance Z_c and propagation constant k are determined as:

$$Z_c = \sqrt{\rho_{eq} K_{eq}} \quad (3)$$

$$k = \omega \sqrt{\rho_{eq} / K_{eq}} \quad (4)$$

The surface impedance Z_s is calculated as:

$$Z_s = -iZ_c \cot(k t) \quad (5)$$

Finally, the normal incidence sound absorption coefficient α is calculated by:

$$\alpha = 1 - \left| \frac{Z_s - \rho_0 c_0}{Z_s + \rho_0 c_0} \right|^2 \quad (6)$$

To determine the sound absorption coefficient of porous materials, Eqs (1-6) require thickness t and five acoustic parameters, which are porosity φ , airflow resistivity σ , tortuosity factor α_∞ , viscous characteristic length Λ , and thermal characteristic length Λ' . The surface acoustic impedance and sound pressure were calculated using the COMSOL software based on the model. First, three cylinders with a bottom diameter of 1 cm and a height of 1 cm were modeled for PAN/CNC, PS/PA66, and PCPP, respectively. Following that, five parameters are necessary to determine the absolute acoustic pressure of FCNS: porosity (φ), flow resistance (σ), viscous characteristic length (Λ), thermal characteristic length (Λ'), and curvature factor (α_∞). Supplementary **Table S2** displays the five parameters that were determined in advance.

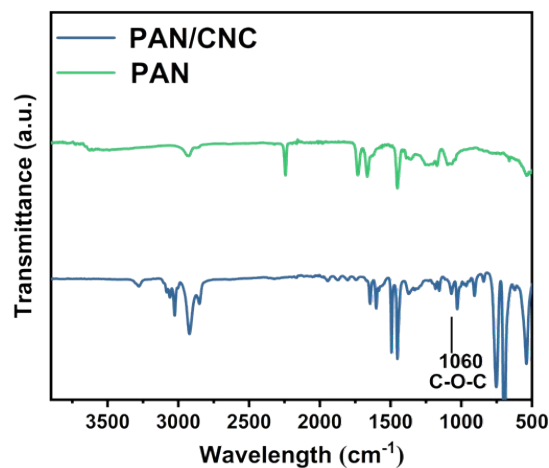


Fig. S1 FTIR spectrum of PAN/CNC and PAN.

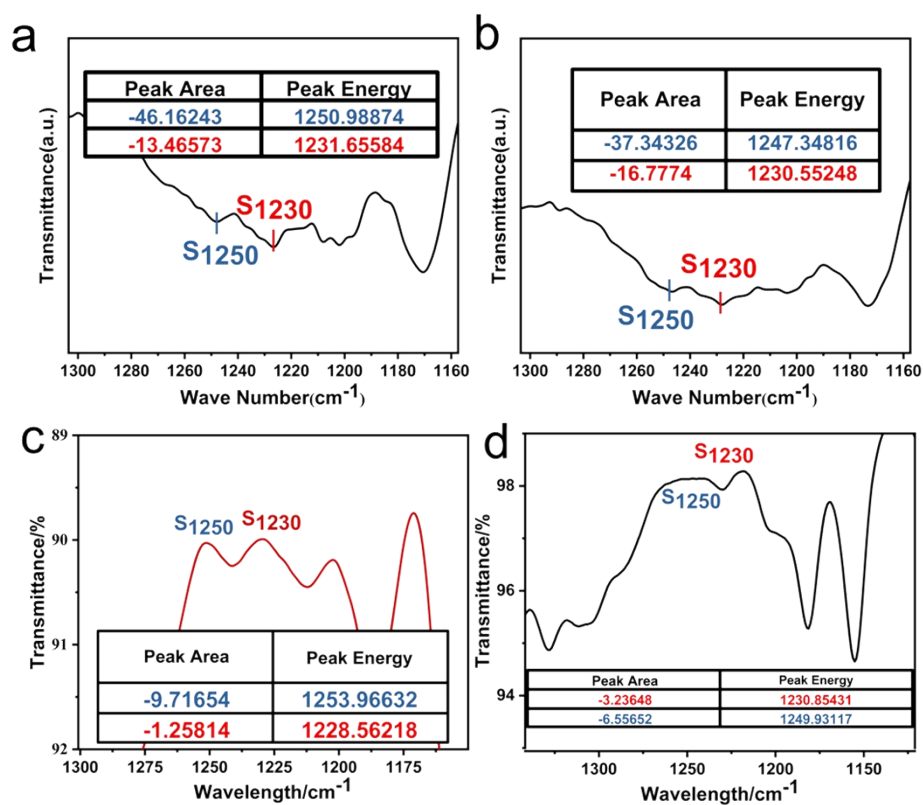


Fig. S2 Peak area at 1230 and 1250 in FTIR spectra (a) CNC content 4% (b) CNC content 2% (c) CNC content 8% (d) CNC content 0%.

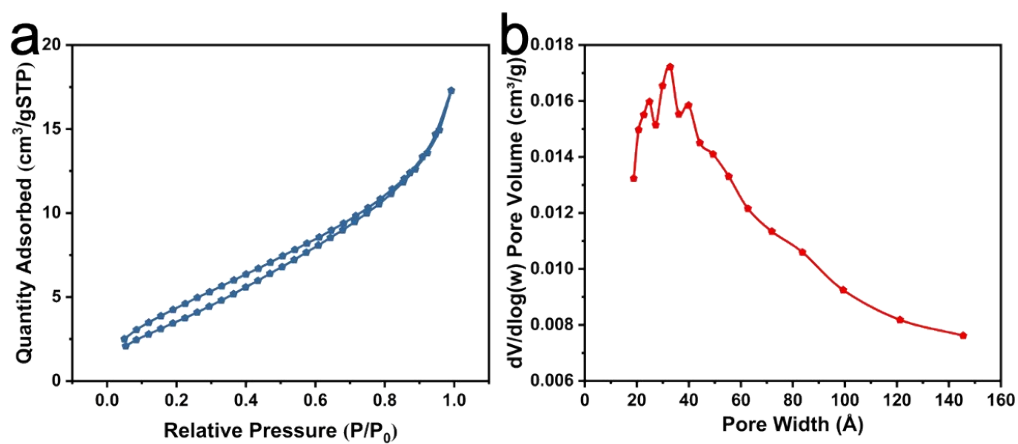


Fig. S3 (a) N_2 adsorption and desorption curve of PAN/CNC. (b) Aperture distribution.

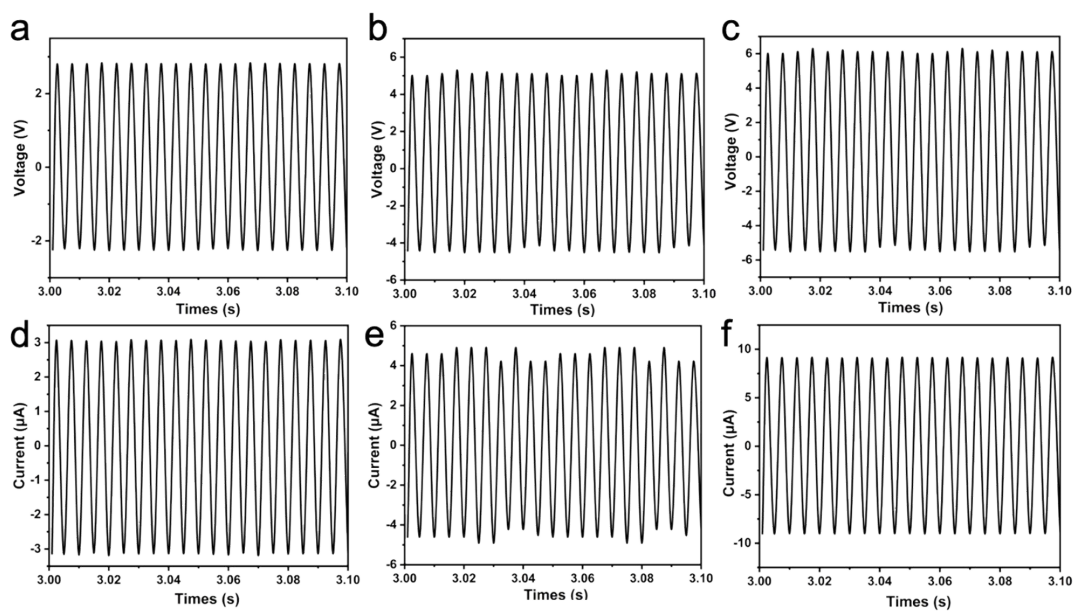


Fig. S4 (a-c) Open Circuit Voltage (2, 4, 8%). (d-f) Short circuit current (2, 4, 8%).

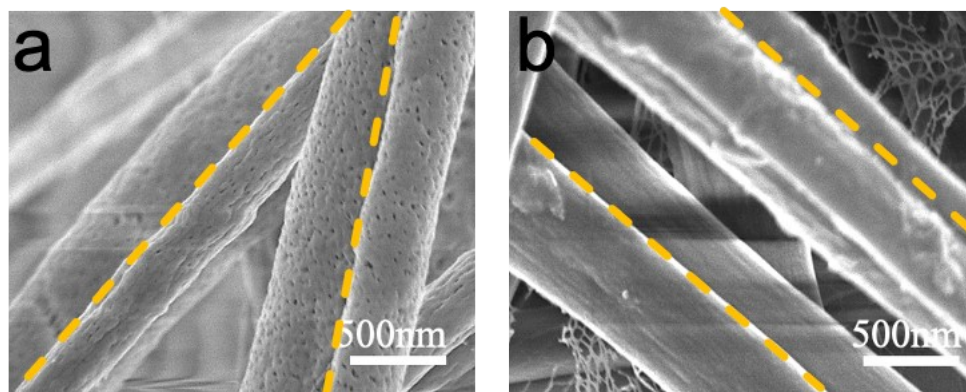


Fig. S5 SEM image of PS/PA66 (a) S_2 and (b) S_3 .

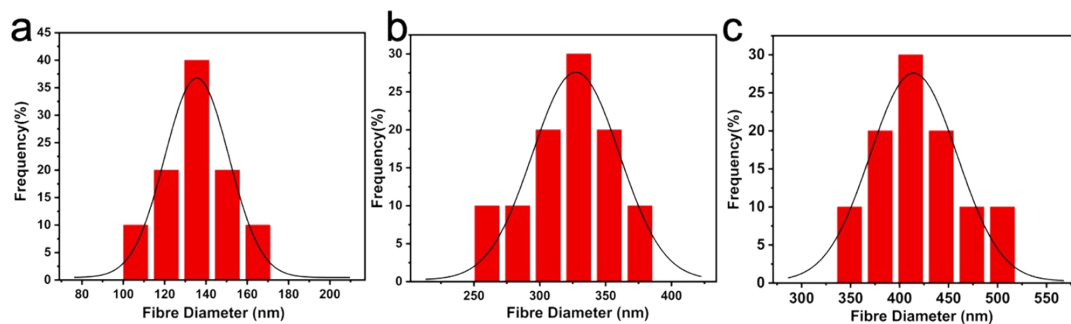


Fig. S6 Fiber diameter distribution of PS/PA66 (a) 1# (b) 2# (c) 3#.

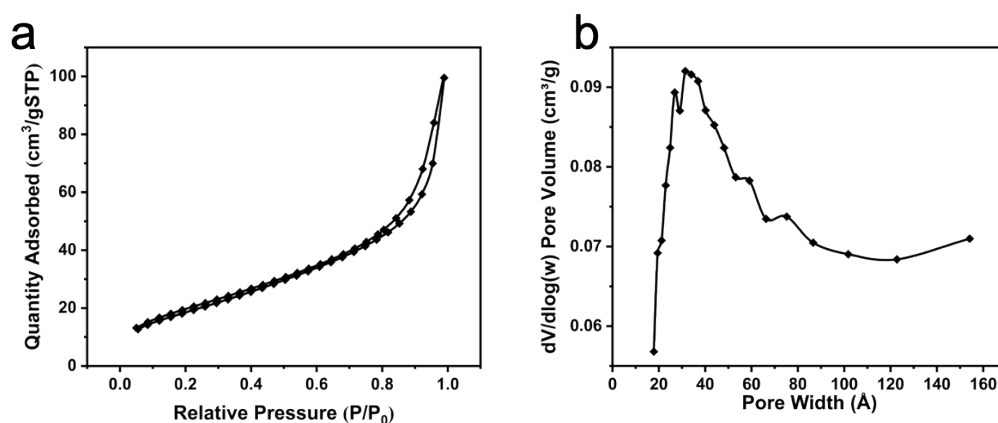


Fig. S7 PS/PA66 (a) N_2 adsorption and desorption curve. (b) Aperture distribution.

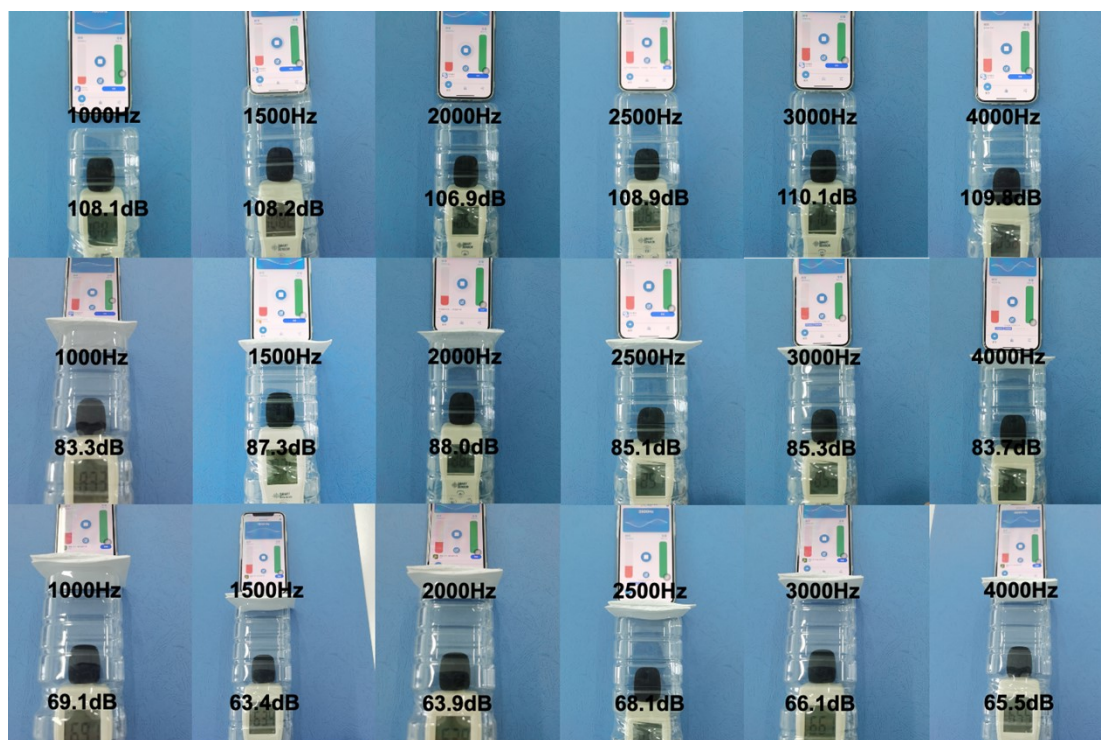


Fig. S8 Sound pressure level test diagram.

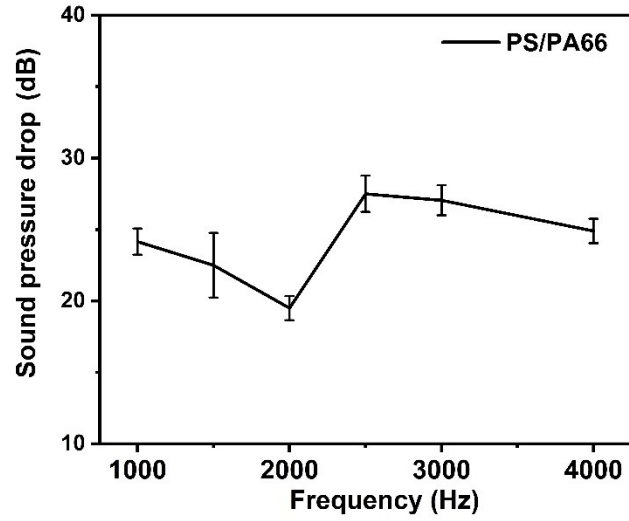


Fig. S9 Sound pressure drops of the PS/PA66 membrane at different frequencies.

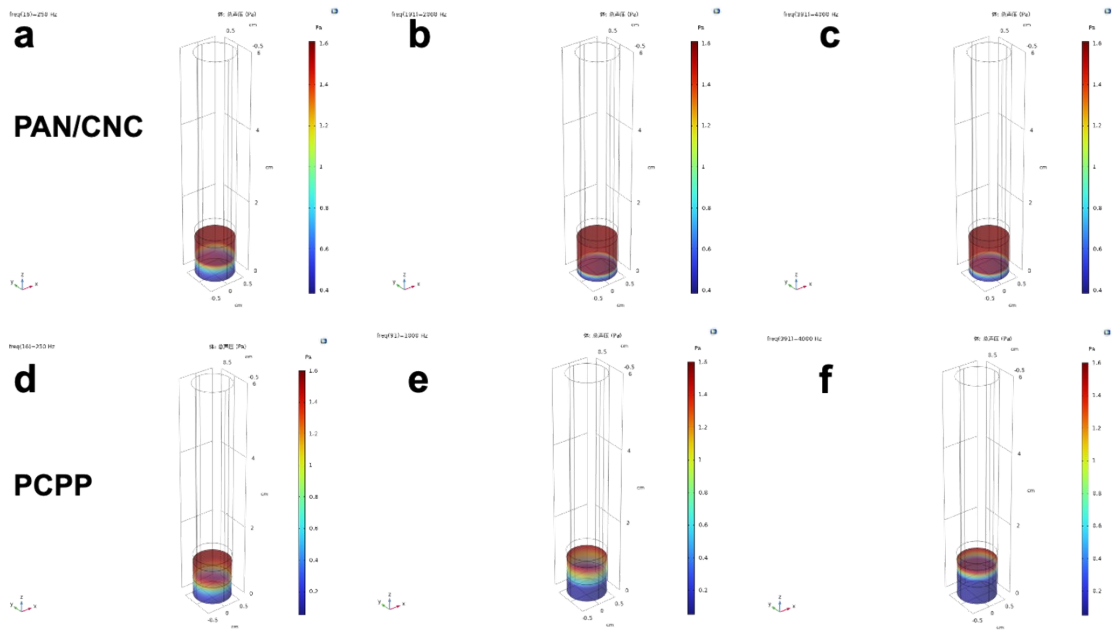


Fig. S10 Comsol simulation test of PAN/CNC below (a) 250Hz, (b) 2000Hz, (c) 4000 Hz. PCPP below (d) 250 Hz, (e) 1000 Hz and (f) 4000 Hz.

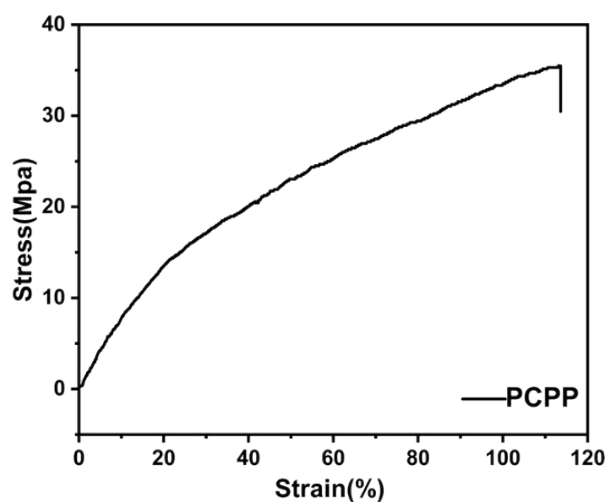


Fig. S11 PCPP Stress-strain curve.

Table S2 Zigzag conformational content.

CNC content	Zigzag conformation content
0%	55.59%
2%	69.00%
4%	77.42%
6%	89.99%
8%	88.54%

Table S3 Zigzag conformational content in other literature.

Raw materials	Treatment	Serrated conformation content	Ref.
PAN	Electrostatic spinning	79.7%	12
PAN/ZNO	In-situ growth	51.55%	13
PAN/PVDF	Electrostatic spinning	86.0%	14
PAN	Electrostatic spinning	81.8%	15
PAN/CNC	Electrostatic spinning	89.9%	This work

Table S4 Acoustic characteristic parameters of PAN/CNC, PS/PA66.

Materials	φ (%)	σ (Pa s m ⁻²)	Λ (μ m)	Λ' (μ m)	α_{∞}
PAN/CNC	94.52	11.2473*e ⁵	26.28	18.32	1.003
PS/PA66	99.33	13.0476*e ⁵	48.31	26.58	1.001

Supplementary References

- 1 M. J. Abraham, T. Murtola, R. Schulz, S. Páll, J. C. Smith, B. Hess and E. Lindahl, *SoftwareX*,

- 2015, **1–2**, 19–25.
- 2 W. Humphrey, A. Dalke and K. Schulten, *J. Mol. Graph.*, 1996, **14**, 33–38.
 - 3 L. Martínez, R. Andrade, E. G. Birgin and J. M. Martínez, *J. Comput. Chem.*, 2009, **30**, 2157–2164.
 - 4 J. Wang, R. M. Wolf, J. W. Caldwell, P. A. Kollman and D. A. Case, *J. Comput. Chem.*, 2004, **25**, 1157–1174.
 - 5 P. Han, W. Nie, G. Zhao and P. Gao, *J. Mol. Liq.*, 2022, **366**, 120243.
 - 6 M. Yabe, K. Mori, K. Ueda and M. Takeda, *J. Comput. Chem., Japan -International Edition*, 2019, **5**, n/a.
 - 7 A. W. Sousa da Silva and W. F. Vranken, *BMC Res Notes*, 2012, **5**, 1–8.
 - 8 P. Li, B. P. Roberts, D. K. Chakravorty and K. M. Merz, *J. Chem. Theory Comput.*, 2013, **9**, 2733–2748.
 - 9 B. Hess, H. Bekker, H. J. C. Berendsen and J. G. E. M. Fraaije, *J. Comput. Chem.*, 1997, **18**, 1463–1472.
 - 10 J. Allard and Y. Champoux, *J. Acoust. Soc. Am.*, 1992, **91**, 3346–3353.
 - 11 N. Kino and T. Ueno, *Appl. Acoust.*, 2007, **68**, 1468–1484.
 - 12 W. Wang, Y. Zheng, X. Jin, Y. Sun, B. Lu, H. Wang, J. Fang, H. Shao and T. Lin, *Nano Energy*, 2019, **56**, 588–594.
 - 13 Y. Sun, Y. Liu, Y. Zheng, Z. Li, J. Fan, L. Wang, X. Liu, J. Liu and W. Shou, *ACS Appl. Mater. Interfaces*, 2020, **12**, 54936–54945.
 - 14 H. Shao, H. Wang, Y. Cao, X. Ding, R. Bai, H. Chang, J. Fang, X. Jin, W. Wang and T. Lin, *Nano Energy*, 2021, **89**, 106427.
 - 15 H. Shao, H. Wang, Y. Cao, X. Ding, J. Fang, H. Niu, W. Wang, C. Lang and T. Lin, *Nano Energy*, 2020, **75**, 104956.